Modal Acoustic Velocimetry in libration-driven flows - Part 1 : Acquisition strategies

Henri-Claude Nataf[1*†], Philippe Roux[1†], Sylvie Su[2†], Philippe Cardin[1], David Cébron[1], Yann Do[1]

[2*]Univ. Grenoble Alpes, CNRS, IRD, Univ. Gustave Eiffel, ISTerre, 38000, Grenoble, France.
[2] Normandie Univ, UNIROUEN, INSA Rouen, CNRS, CORIA, 76000, Rouen, France.

*Corresponding author(s). E-mail(s): Henri-Claude.Nataf@univ-grenoble-alpes.fr;
Contributing authors: Philippe.Roux@univ-grenoble-alpes.fr; sylvie.su@univ-rouen.fr; Philippe.Cardin@univ-grenoble-alpes.fr; David.Cebron@univ-grenoble-alpes.fr; Yann.Do@univ-grenoble-alpes.fr;
†These authors contributed equally to this work.

Abstract

Modal Acoustic Velocimetry was introduced by Triana et al. (2014) as a new method inspired from helioseismology for probing fluid flows. Acoustic modes are excited in a spinning fluid-filled spheroid. Rotation and fluid flow modify the characteristics of these modes, lifting the degeneracy of non-axisymmetric modes. So far, this method has only been applied to stationary or statistically stationary flows, by measuring frequency splittings in the spectral domain. Here, we develop strategies to probe libration-induced flows. One strategy operates in the frequency domain and relies on the periodicity of the flow, while the other one rests on a high-resolution algorithm in the time domain. The retrieved mode frequency splittings are compared to those computed for an asymptotic libration-induced flow (Greenspan 1968), validating both our strategies. Inversion of these splittings to retrieve fluid flow is presented in a companion article (Nataf and Su 2025).

Keywords: Modal Acoustic Velocimetry, libration, spheroid, acoustics

1 Introduction

This article describes acquisition strategies developed to apply Modal Acoustic Velocimetry for flows produced by longitudinal libration in a rapidly spinning gas-filled spheroid. These strategies are implemented in the ZoRo experiment. The basics of Modal Acoustic Velocimetry are recalled in this introduction, together with a brief description of libration-induced flows, a presentation of the ZoRo setup, and a reminder about acoustic modes. Two acquisition strategies are presented in section 2. Resulting experimental results are compared with theoretical predictions in section 3. Section 4 discusses the limitations and perspectives of our study, and we conclude in Section 5. A companion article (Nataf and Su 2025) deals with the inversion of the data presented in this study and presents maps of the retrieved flows.

1.1 Modal Acoustic Velocimetry

Modal Acoustic Velocimetry (MAV) was introduced by Triana et al. (2014) as a new method to measure flow velocity in fluid-filled cavities. It is inspired by helioseismology and proves useful in experiments where tracers cannot be employed, such as in rapidly rotating spheres or spheroids (Triana et al. 2014; Mautino 2016; Su et al. 2020; Su 2020; Vidal et al. 2020). The method consists in exciting the acoustic normal modes of the fluid in the cavity, and measuring for each mode the frequency shift induced by solid body rotation and fluid flow. Previous works (Triana et al. 2014; Mautino 2016; Su et al. 2020; Su 2020) focused on stationary or statistically stationary flows. Acoustic modes can then be excited by long-lasting chirps, covering a wide frequency range and providing a fine frequency resolution. In this article, we report on strategies we developed to apply MAV on non-stationary flows, focusing on time-periodic flows induced by libration.

1.2 Libration

Libration-induced flows in rapidly-rotating spheres and spheroids have received a lot of attention because of their geophysical and planetary relevance (Aldridge 1967; Tilgner 1999; Comstock and Bills 2003; Noir et al. 2009; Busse 2010; Le Bars et al. 2015; Cébron et al. 2021). For longitudinal libration, the instantaneous rotation frequency $f_{shell}(t)$ of a gas-filled shell can be written as:

$$f_{shell}(t) = f_o + \Delta f \sin(2\pi f_{lib} t), \tag{1}$$

where f_o, Δf, and f_{lib} denote the average shell rotation rate, libration amplitude, and libration frequency, respectively. We will only consider cases with $\Delta f \ll f_o$ and $f_{lib} \ll f_o$, allowing to neglect non-linear effects and the harmonic modulation of the boundary-layer flow, respectively.

This shell motion can be regarded as a continuous succession of infinitesimal spin-up and spin-down forcings, which have been studied in detail by Greenspan and co-workers (Greenspan and Howard 1963; Greenspan 1968).

In the asymptotic regime corresponding to rapid rotation and small libration amplitude, the induced flow obeys Proudman-Taylor constraint, and is thus z-independent

(where z marks the coordinate along the rotation axis) except in a thin viscous boundary layer beneath the shell, the Ekman layer.

In an axisymmetric shell spinning around its symmetry axis, fluid flow is then a function of cylindrical radius and time only. Following Deleplace (2005, p.42-46), the fluid rotation rate $f_{fluid}(s,t)$ in the rotating frame is then obtained as

$$\frac{f_{fluid}(s,t)}{\Delta f} = \frac{\xi}{\sqrt{1+\xi^2}} \sin\left(2\pi f_{lib}\, t + \pi + \arctan\frac{1}{\xi}\right), \tag{2}$$

where the expression of ξ depends on the geometry of the shell. For a sphere of radius r_o, it is given by

$$\xi = \frac{f_{lib}}{f_{Ekman}} (1-s^2)^{3/4}, \tag{3}$$

where s is the cylindrical radius, normalized by r_o and

$$\frac{f_{Ekman}}{f_o} = \sqrt{\frac{2\pi\nu}{f_o r_o^2}} = 2\pi \mathrm{Ek}^{1/2},$$

where ν is the kinematic viscosity of the fluid, and $\mathrm{Ek} = \nu/(2\pi f_o r_o^2)$ is the Ekman number. The expression for an axisymmetric spheroid is derived in Appendix A.

Figure 1 shows the fluid rotation rate predicted for $f_{lib}/f_{Ekman} = 0.266$, which corresponds to $f_{lib} = 0.05$ Hz for the ZoRo experiment filled with air at normal conditions ($\nu = 1.5 \times 10^{-5}$ m^2 s^{-1}), spinning at $f_o = 15$ Hz. Dimensionless fluid flow rotation rate $f_{fluid}(s,t)/\Delta f$ is contoured in an s-t map, with time t normalized by $T_{lib} = 1/f_{lib}$.

Another representation is proposed in Figure 2, where s-profiles of the fluid rotation rate (in the librating shell frame) are shown at different libration phases every 36° from 0° to 324°. Crosses give the same quantities as measured in the equatorial plane of an axisymmetric numerical simulation performed in the spherical geometry, using the XSHELLS package (Schaeffer 2013; Kaplan et al. 2017), with $\Delta f = 1.5$ Hz and $\mathrm{Ek} = 4 \times 10^{-6}$. The differences between the finite amplitude numerical simulation and the analytical asymptotic expression are very small in this parameter range. For large libration amplitudes Δf, longitudinal rolls develop in the Ekman boundary layer during the spin-down phase of the libration cycle (Noir et al. 2009). These rolls are clearly observed in axisymmetric numerical simulations when increasing Δf to 3.6 Hz.

In this article, we restrict our attention to the stable regime for which Greenspan's asymptotic theory provides an excellent flow prediction. This is the type of time-periodic flow that we produced and analyzed in our ZoRo experiment, which we now describe.

1.3 The ZoRo experiment

The ZoRo experiment was set-up to investigate convective and mechanically induced flows in a rapidly rotating gas-filled spheroid. Such flows are observed or expected in the fluid enveloppes of planets. The experiment consists in an aluminum shell that can

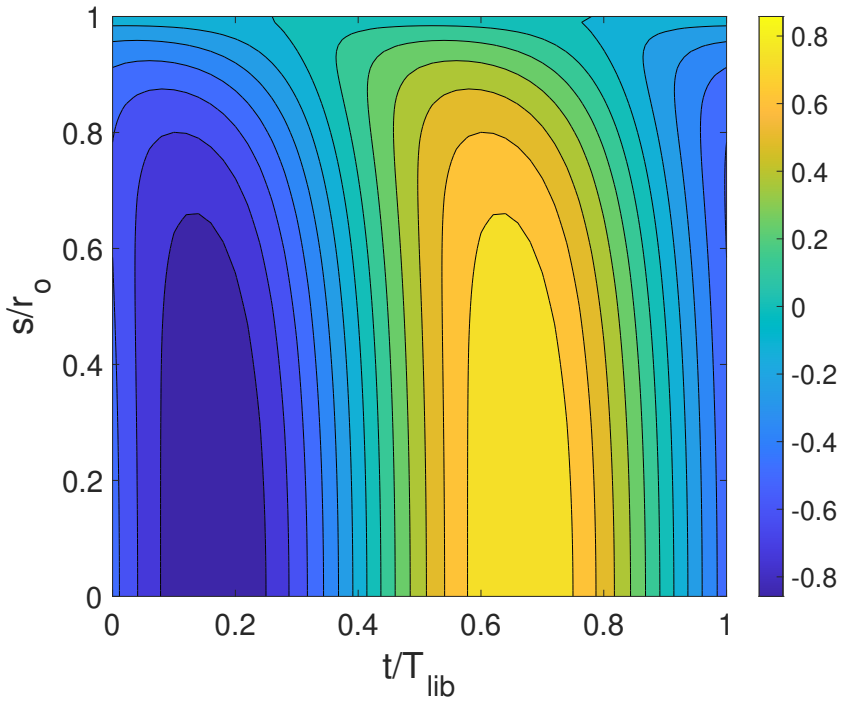

Fig. 1 Isocontours of fluid rotation rate as a function of time and cylindrical radius, as predicted by Greenspan's theory for libration in a rapidly spinning sphere, with $f_{lib}/f_{Ekman} = 0.266$. Fluid rotation rate is expressed in the spinning shell reference frame, and normalized by Δf. Cylindrical radius and time are normalized by r_o and T_{lib}, respectively.

spin around a vertical axis at rates up to 50 rotations per second. The shell can be filled with different gases (air, nitrogen, argon) kept at pressures between 0.3×10^5 and 4×10^5 Pa. The axisymmetric cavity has an equatorial radius $r_{eq} = 0.2$ m and polar radius $r_{pol} = 0.19$ m. A sphere of the same volume has radius $r_o = \sqrt[3]{r_{eq}^2 r_{pol}} = 0.1966$ m.

The MAV technique was implemented in ZoRo since strong centrifugal effects disqualify tracer-based techniques. The rotating shell is thus equipped with four loudspeakers and fourteen microphones. Su et al. (2020) describe the methodology developed to excite, measure, model, and process the acoustic modes of ZoRo. They also show measurements of acoustic mode splitting caused by the Coriolis force in solid body rotation, confirming the theory of Ledoux (1951). More details can be found in Su et al. (2020) and Su (2020).

Libration is produced by varying the instantaneous spin rate of the shell with time in a sinusoidal fashion. Particular care is given to the synchronization of the various measurements (see Appendix B for details). In ZoRo, the libration flow shown in Figure 1 is obtained with $f_o = 15$ Hz and $f_{lib} = 0.05$ Hz, when it is filled with air at ambient pressure and temperature ($\nu = 1.5 \times 10^{-5}$ m^2 s^{-1}). The Ekman number is

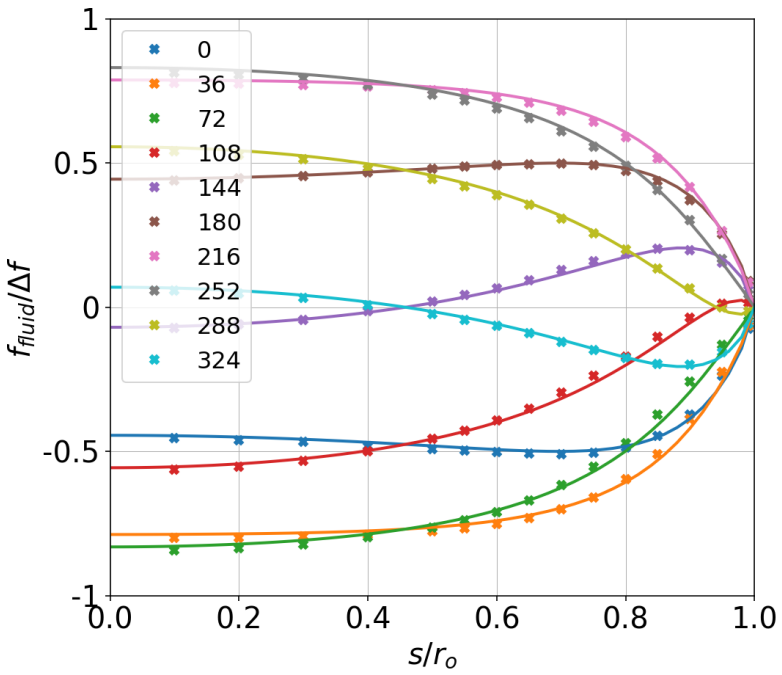

Fig. 2 Same libration flow as in Figure 1, with $f_o = 15$ Hz, $f_{lib} = 0.05$ Hz and $\Delta f = 1.5$ Hz. Solid lines show fluid rotation rate as a function of cylindrical radius from Greenspan's theory, for selected libration phases from 0° to 324° in 36°-steps. Crosses are the corresponding fluid rotation rates measured in the equatorial plane of an axisymmetric numerical simulation ($\mathrm{Ek} = 4 \times 10^{-6}$).

then $\mathrm{Ek} = 4 \times 10^{-6}$, yielding $f_{Ekman} = 0.188$ Hz, and the exponential thickness of the viscous layer beneath the shell, called the Ekman layer, is $\delta_{Ekman} = \sqrt{\nu/(2\pi f_o)} = 0.4$ mm.

1.4 Acoustic modes

We briefly recall here a few basic properties of acoustic modes in a gas-filled spheroid (more details in (Ledoux 1951; Moldover et al. 1986; Mehl 2007; Aerts et al. 2010; Triana et al. 2014; Su et al. 2020; Vidal et al. 2020)). Starting from a full sphere, we recall that acoustic modes are quantized. The pressure field of a resonant acoustic mode can we written as:

$$p(r, \theta, \phi) = {}_nR_l(r)\, Y_l^m(\theta, \phi), \tag{4}$$

where $Y_l^m(\theta, \phi)$ is the spherical harmonic of degree l and order m, which describes the surface variation of the mode's pressure field. Index n gives the number of zeroes of function ${}_nR_l(r)$, which provides the radial variation of the mode's pressure field, and is given by ${}_nR_l(r) = j_l({}_nk_l\, r)$, where j_l is the spherical Bessel function of the first kind, of degree l, and ${}_nk_l$ is such that, for a rigid shell, ${}_nR_l'|_{r=1} = 0$, where the prime represents the r-derivative. Each mode resonates at a specific frequency ${}_nf_l^m$.

In a sphere of radius r_o, frequencies are m-degenerate: ${}_nf_l^m = {}_nf_l = {}_nk_l\, c/(2\pi r_o)$ for all m, with c the sound velocity of the gas.

In a spheroid, this m-degeneracy is partly lifted, but *doublets* ${}_nS_l^{\pm m}$ still have the same frequency. Global rotation and/or azimuthal flows lift this remaining degeneracy. MAV thus measures the frequency difference between *singlets* ${}_nS_l^{-m}$ and ${}_nS_l^m$ to retrieve global axisymmetric maps of azimuthal flow velocity.

Following Su et al. (2020), we compute predicted mode frequencies ${}_nf_l^m$ by perturbation theory to the second order in ellipticity, in order to obtain the right ordering of the doublets. Note that we the projection on spherical harmonics is an approximation in the spheroidal case, and only applies for moderate flattening. See Su et al. (2020) for details, and Vidal et al. (2020) for a more complete and rigorous presentation. One limitation of the shape perturbation theory we use (Mehl 2007) is that it does not provide the eigen function perturbation. However, the flattening of ZoRo is small enough that using the spherical eigen modes is appropriate. A method for computing pressure fields at higher-order in ellipticity is presented in Albo et al. (2010).

2 MAV strategies for time-periodic flows

Previous MAV exercises (Triana et al. 2014; Mautino 2016; Su et al. 2020) excited acoustic modes by playing long chirps covering a large frequency range, and retrieved mode frequencies from the Fourier transform of the recorded signals. This strategy is well fit for stationary flows or for retrieving the mean of a moderately fluctuating flow. For time-varying flows such as those generated by libration, one would like to capture acoustic signatures in a short time lapse, of the order of a second for the case shown in Figure 1. From Nyquist's theorem, frequency resolution would then be of the order of one Hertz.

However, we will see that these flows produce mode splittings that typically range from 0.5 Hz to 15 Hz. This suggests that a frequency resolution of 1 Hz is not sufficient to properly constrain the flow. Faced to this problem, we developed and tested two strategies, which we now present.

2.1 Long chirps repeated with a libration phase offset

Our first strategy is to play and record long chirps (typically ~ 90 seconds) covering the full frequency range (500 to 5 000 Hz) we can access. We thus obtain Fourier power spectra with a resolution of the order of 0.01 Hz. Of course, flow evolves while the chirp is played, but a given mode is only excited at a given time, or rather during a short time lapse (typically less than 0.2 to 1 second). Keeping track of the evolution of libration phase during the chirp, the measured splitting of a given mode can then be attributed to a known libration phase. By repeating the same chirp at different initial libration phase we scan the evolution of each mode splitting with libration phase.

An example is shown in Figure 3. Libration parameters are $f_o = 15$ Hz, $f_{lib} = 0.05$ Hz and $\Delta f = 1.5$ Hz, and we play an 82s–long chirp spanning from 500 to 5 000 Hz. This chirp is repeated 10 times. During one chirp, the setup experiences 4.1 libration periods. Successive chirps thus sample the libration flow with a phase shift of 36°.

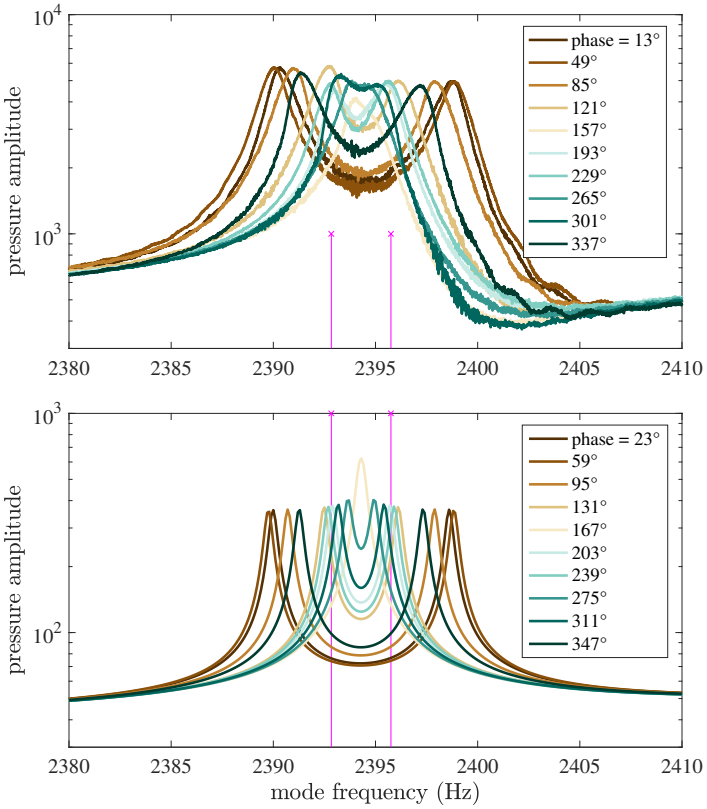

Fig. 3 Frequency spectra of split acoustic doublet ${}_1S_3^{\pm 3}$ for 10 successive libration phases, 36° apart. Libration parameters : $f_o = 15$ Hz, $f_{lib} = 0.05$ Hz and $\Delta f = 1.5$ Hz. (a) measured power spectra. The plot is a zoom centered at 2395 Hz of full spectra obtained by playing a 82s–long chirp spanning from 500 to 5 000 Hz. The legend indicates the libration phase achieved by the setup when the center frequency is played. (b) synthetic spectra computed from the splitting predicted by the convolution of the acoustic sensitivity kernel with Greenspan's libration flow model. Note that a phase delay of 10° has been added to the synthetics as compared to the measured data. The two magenta stems mark the frequencies of the ${}_1S_3^3$ and ${}_1S_3^{-3}$ singlets for solid body rotation of the fluid with the shell at spin rate f_o.

We compute the power spectrum of the signals recorded for each of the ten 82s–long chirps.

Figure 3a displays a zoom of the ten spectra focused on acoustic doublet ${}_1S_3^{\pm 3}$. As in Su et al. (2020), each spectrum is obtained following these steps: (i) since this doublet is equatorially symmetric (because $l-m$ is even), we first sum the time-records of pairs of equatorially symmetric microphones; (ii) we compute the power spectrum

of three such summed time-records; (ii) we take the mean of these three power spectra. The libration phase of each mean power spectrum, as listed in the legend, is deduced from the time $t - t_0$ at which the central frequency of the doublet is played in the chirp, t_0 corresponding to a nul libration phase.

Figure 3b shows synthetic power spectra computed for the same libration phases, augmented by a 10° delay (for reasons to be discussed later). Each spectrum is built following these steps: (i) the theoretical frequencies of the ${}_1S_3^3$ and ${}_1S_3^{-3}$ singlets are obtained by convolving the acoustic velocity kernel with the theoretical libration-flow model of equation 2 for the considered libration phase $2\pi f_{lib}(t - t_0)$; (ii) the acoustic power spectrum is computed by convolving each singlet's resonance lines with a Lorentzian (Su et al. 2020).

In this figure, the largest splitting is obtained for a libration phase of 59°. From Figures 1 and 2, we see that the fluid rotation rate (in the spinning shell frame) is retrograde and near its minimum at that phase. The splitting decreases as the libration phase increases, until a phase of 167° when a single frequency peak is observed. This occurs when the splitting due to the fluid flow exactly cancels the splitting due to the shell spin, which is indicated by the two magenta stems for a $f_o = 15$ Hz spin rate. As the fluid flow becomes positive (prograde) the two singlets cross each other, yielding a splitting that increases again to a secondary maximum at a phase of 347°.

The exact same evolution is observed in Figure 3a, with almost identical amplitudes. The main difference is the width of the resonance peaks, which is larger than expected from the theory, some widening being probably due to the evolution of the flow during the resonance buildup.

Our phase-offset long chirp strategy then consists in measuring the frequency splitting of as many doublets as possible for ten successive libration phases.

For each doublet, the splitting estimate and its error bar are obtained with the following steps (Su et al. 2020): (i) 'plus' and 'minus' time-records are obtained from the sum and difference of sound recorded by four pairs of equatorially-symmetric microphones (${}_nS_l^{\pm m}$ doublets with even $l - m$ show up in 'plus' records, while those with odd $l - m$ are seen in 'minus' records); (ii) 'plus' and 'minus' records are Fourier transformed; (iii) the resulting four 'plus' power spectra are averaged yielding 'mean+' power spectrum, and 'mean-' is obtained similarly; (iv) doublets ${}_nS_l^{\pm m}$ are identified in these spectra with the help of synthetic spectra, and a windowed spectrum is extracted together with a first estimate of mode splitting; (v) individual synthetic spectra are built varying four of their constitutive ingredients: doublet's peak-to-peak splitting, doublet's mean frequency, doublet's amplitude, and singlets' peak width; (vi) a grid search on these four elements provides the best splitting and its error bar.

This strategy only applies to time-periodic flows and requires that the played chirp largely dominates over other noise sources.

2.2 Short chirps and high-resolution frequency analysis

We developed a second strategy: play a short chirp centered on the frequency of a single acoustic doublet. Fluid rotation splits this doublet into two singlets with slightly different frequencies. The time-domain record of a given microphone thus consists in

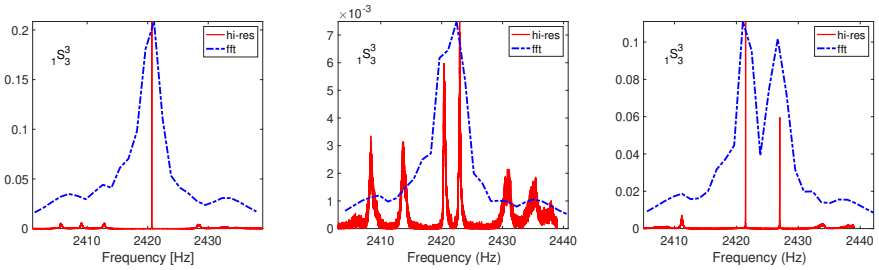

Fig. 4 Examples of the high-resolution analysis. Histograms (in red) of frequencies recovered by the iterative IRWIN algorithm for doublet ${}_1S_3^3$ at three different libration phases. The dot-dashed blue line gives the standard Fourier spectrum computed for each 0.82s-long time window.

the superposition of two sine signals with slightly different periods. A one second-long record contains thousands of cycles, enough to detect and measure the two frequencies with a precision of 0.01 Hz. In other words, while obtaining the full frequency spectrum is limited by Nyquist theorem, this limit vanishes when the signal consists in the sum of a small number of sines that we wish to retrieve.

Processing follows a variant of the IRWIN method presented by Roux et al. (2004) and Philippe et al. (2008). The main ingredients of this method is recalled in Appendix D. For our application, the following steps are taken: (i) a short chirp (lasting typically less than 1 second) is repeatedly played on one or two loudspeakers, covering the resonance frequency range of a targeted doublet. (ii) we compute the auto-correlation of each record. (iii) we choose the number of monochromatic components to be searched for, and the frequency interval for the search. (iv) we launch an ensemble of inversions. (v) we gather the results in histograms that count the number of times each frequency has been recovered in the ensemble. One or two peaks normally stand up, yielding the singlets' frequencies and their error bar. (vi) the procedure is repeated for the following chirps, probing successive phases pf the libration-induced flow.

Figure 4 illustrates the performance of our high-resolution algorithm for three different libration phases for doublet ${}_1S_3^{\pm 3}$. While Nyquist theorem limits the frequency resolution of the standard power spectrum (dot-dash blue line) of our 0.82s-long time window, the high-resolution algorithm (red) isolates one or two frequencies very precisely in the time-domain signals. The middle panel shows a case when the algorithm only marginally recovers the frequencies.

The main limitation of this technique is that only a limited number of doublets can be targeted at the same time. We obtained good results with up to four simultaneous doublets, but the examples shown below target a single doublet. One advantage of this method is that it can be used to probe non-periodic time-varying flows.

3 Comparing observations and synthetics

We give here examples of measurements obtained with both strategies. The data are compared with predictions computed by convolving the time-dependent fluid flow with the kernel of each acoustic mode. Fluid flow $f_{fluid}(s,t)$ is computed using the linear geostrophic theory of Greenspan and Howard (1963) adapted to libration in a spheroid,

namely from equations (2) and (A2). Note that we often replace time t by the libration phase $\phi(t) = 2\pi f_{lib}\, t \bmod 2\pi$. The acoustic kernel ${}_n\mathbb{K}_l^m(s)$ provides the frequency splitting $\delta f_{{}_nS_l^{\pm m}}(t)$ of acoustic doublet ${}_nS_l^{\pm m}$ (see definition and expression in Nataf and Su (2025)). Note that although we compute mode frequencies by perturbation theory to second-order in ellipticity (Su et al. 2020), we use the acoustic kernels of a sphere.

3.1 Mode splitting collection from phase-offset chirps

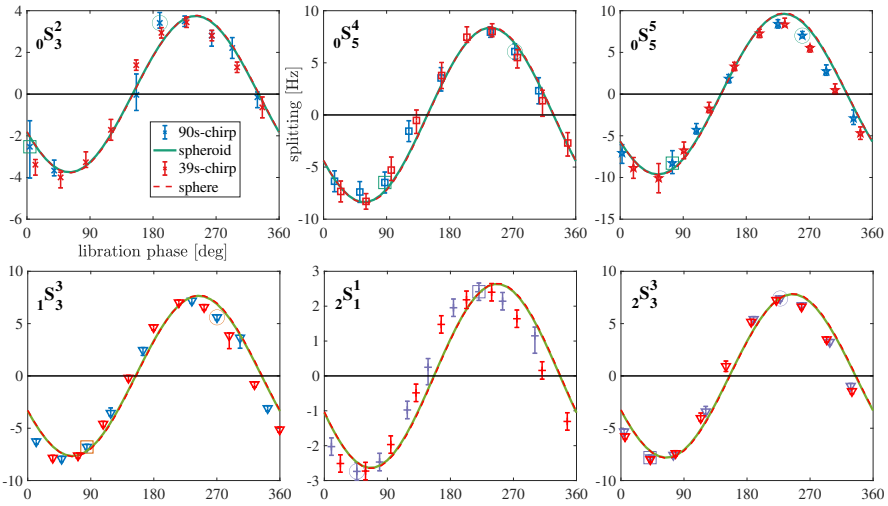

Fig. 5 Peak-to-peak frequency splitting in Hz as a function of libration phase for six selected acoustic doublets ${}_nS_l^{|m|}$. Data points with error bars are measured in the ZoRo experiment librating with $f_o = 15$ Hz, $f_{lib} = 0.1$ Hz and $\Delta f = 1.5$ Hz. Phase-offset chirps with two different durations were used: 90s (blue) and 39s (red) Splittings predicted from Greenspan's theory are drawn for ZoRo's spheroid (solid line) and for the sphere (dashed line), which plot on top of each other.

We could measure the frequency splittings of some 53 doublets with the phase-offset long chirps strategy. Figure 5 compares results obtained for two chirp durations: 90 and 39 seconds. Libration parameters are: $f_o = 15$ Hz, $f_{lib} = 0.1$ Hz and $\Delta f = 1.5$ Hz. For each selected acoustic doublet ${}_nS_l^{\pm m}$, the measured splitting (frequency difference between spectral peaks of ${}_nS_l^{-m}$ and ${}_nS_l^{+m}$ singlets) is plotted as a function of libration phase. All splittings are first corrected for the effect of the Coriolis force computed at the rotation rate of the shell $f_{shell}(t)$. We use the Ledoux coefficients of Vidal et al. (2020) computed for ZoRo's flattening, but the difference with the spherical Ledoux coefficients is negligible except for the lowest frequency fundamental modes. The measurements are compared to the splittings predicted by the libration flow model for a spheroid (solid line) and for a sphere (dashed line), which are almost perfectly superposed. The signature of the time-varying libration flow is very well retrieved by MAV, but data appear to probe a libration flow that is about 20° further, which

corresponds to a delay of about 0.5s. No significant difference is seen between the two chirp durations. We will get back to the delay problem in section 3.2.

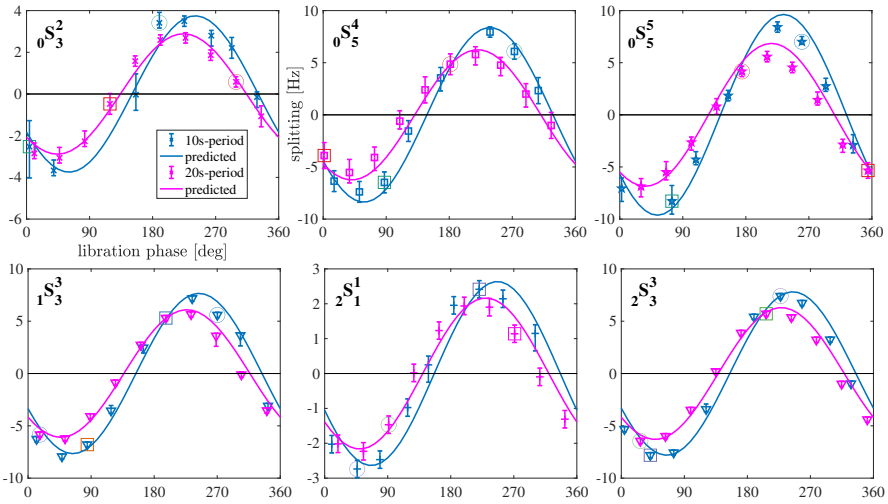

Fig. 6 Frequency splittings for two different libration frequencies: $f_{lib} = 0.1$ Hz (blue) and 0.05 Hz (magenta), both with $f_o = 15$ Hz and $\Delta f = 1.5$ Hz as in Figure 5. Symbols and error bars for measurements with 90s- and 98s-long phase-offset chirps. Sine solid lines for corresponding Greenspan's predictions for ZoRo's spheroid.

Figure 6 compares two cases with different libration frequencies: $f_{lib} = 0.1$ Hz as in Figure 5 versus $f_{lib} = 0.05$ Hz (98 s-long chirp). At smaller libration frequencies, fluid gets toward better synchronisation with shell's rotation rate, implying smaller differential rotation and smaller phase shift between the fluid and the shell. This behaviour is clearly seen in the synthetic curves, and well recovered by MAV.

The splitting evolution with phase libration is shown in Appendix C for all 53 acoustic modes.

3.2 Short chirps results

We tested the short-chirp technique on acoustic doublet $_1S_3^{\pm 3}$. First tests with chirps spanning 2 350 to 2 430 Hz in 4 seconds were performed for a uniform shell rotation, with f_o ranging from 1 to 20 Hz, providing splittings from 0.19 to 3.85 Hz, with error bars of about 0.01 Hz, in excellent agreement with Ledoux coefficients computed by 3^{rd} order-perturbation in ellipticity and rotation rate by Vidal et al. (2020).

The method was then applied to libration flows. Figure 7 shows an example of $_1S_3^{\pm 3}$ doublet's splitting as a function of libration phase. Libration parameters are $f_o = 15$ Hz, $f_{lib} = 0.084$ Hz and $\Delta f = 1.5$ Hz. A succession of 32 identical signals is played. Each signal consists of a 0.37 s-long chirp from 2360 to 2398 Hz, followed by a 0.37 s silence. The signal is played simultaneously by two loudspeakers placed at latitudes $+45°$ and $-45°$ along the same meridian, thus favoring equatorially symmetric modes.

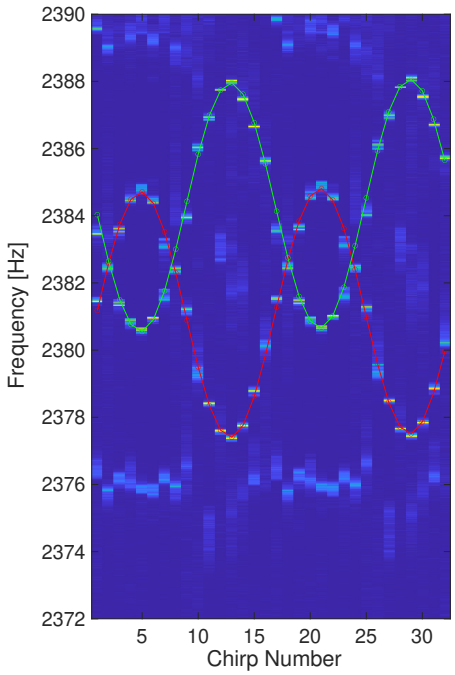

Fig. 7 Splitting example of the short chirps method. Libration parameters: $f_o = 15$ Hz, $f_{lib} = 0.084$ Hz and $\Delta f = 1.5$ Hz. A succession of 32 short chirps centered around the resonant frequencies of the ${}_1S_3^{\pm 3}$ doublet. Each chirp plays frequencies 2 360 to 2 398 Hz in 0.37s and is followed by a silence of equal duration.

The overall sequence covers two libration periods. The resulting record is chopped to recover the response to each individual chirp, and the high-resolution algorithm is applied to each of the 32 extracted time records. The algorithm measures the probability for a given frequency to be present in the record. Figure 7 is a composite plot of the probability maps of all 32 segments. Two frequencies clearly emerge, which follow a sine pattern, thus revealing the variation of the ${}_1S_3^{\pm 3}$ doublet's frequency splitting as a function of libration phase. Note that the two sine curves cross each-other, because the splitting produced by the flow exceeds the Coriolis splitting for this doublet, as in Figure 3.

We now go deeper into the analysis of these measurements. Figure 8 compiles several measurements and predictions for this doublet. We first retrieve the frequency splitting for each chirp from the data of Figure 7, yielding the green solid curve in Figure 8. Note that the resulting sine curve is not centered on the zero line but on the magenta horizontal dash line, which marks the splitting due to solid body rotation at the f_o spin rate (*i.e.,* the Ledoux coefficient times f_o). The green dash-dot curve

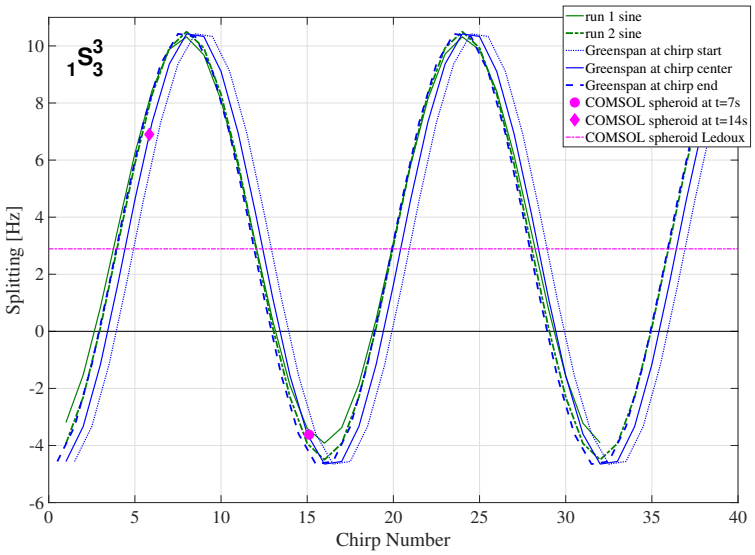

Fig. 8 Comparison between predicted and measured frequency splitting of the ${}_1S_3^{\pm 3}$ doublet. Libration parameters as in Figure 7: $f_o = 15$ Hz, $f_{lib} = 0.084$ Hz and $\Delta f = 1.5$ Hz. The x-axis is time given in chirp number. There are exactly 16 chirps in one libration period. The y-axis is the frequency difference between singlets ${}_1S_3^{-3}$ and ${}_1S_3^{+3}$. The green solid curve is derived from the data of Figure 7. The green dash-dot line is the sine fit of frequencies obtained for another run (see text). The blue solid line gives the frequency splitting predicted by convolving Greenspan's libration flow with the acoustic splitting kernel (for a sphere) of the ${}_1S_3^{\pm 3}$ doublet. The blue dashed and blue dotted lines are the same prediction shifted by -0.37s and 0.37s respectively. The magenta symbols are from a computation taking into account the exact spheroidal geometry of the experiment. The magenta horizontal dash line gives the splitting for solid body rotation at $f_o = 15$ Hz.

is a sine fit of the data obtained in another run, playing a succession of 64 chirps lasting 0.74s (no silence between chirps), from 2 350 to 2 430 Hz. The two curves almost coincide.

Let us compare these data with the splitting expected for this libration flow. The blue solid line gives the time-evolution of the frequency splitting predicted from Greenspan's linear theory, after convolution of the time-dependent fluid flow with the acoustic kernel. The time taken into account for the computation of the flow is the center-time of the 0.74s-long chirp. The blue dotted line instead considers the start-time of the chirp, while the blue dash line considers the end-time of the chirp. We see that the data almost perfectly agree with the latter prediction, both in pattern, in amplitude, and in phase. We conclude that the mode splitting we measure is perfectly consistent with the fluid flow predicted by Greenspan's linear theory. This is in line with the results shown in Figure 2, which show an excellent agreement between that theory and a finite amplitude axisymmetric simulation. However, our measurements confirm a delay of the order of 0.3s between the flow and its acoustic modal response, confirming the observations of section 3.1. We believe that it corresponds to the time for a mode to build up, as detailed in Appendix E.

We checked for another potential bias. The acoustic kernels we use to compute the predicted splittings are for a sphere. Since it was shown by Su et al. (2020) that theory had to be extended to second order perturbations in ellipticity in order to provide a correct ordering of the frequencies of a given multiplet, our simplification could introduce a bias. We checked that this was not the case, at least for the ${}_1S_3^{\pm 3}$ doublet presented here. For that, we ran a simulation of the acoustic response of a ZoRo-like spheroid using the finite-element COMSOL Multiphysics®software, with $f_o = 15$ Hz, imposing Greenspan's flow. The magenta symbols in Figure 8 give the results we obtain for two different libration phases. They plot exactly on the blue solid line, which corresponds to the response of a sphere.

3.3 Combining both strategies

One advantage of the high-resolution method is that it provides a much more precise estimate of the frequency splitting. This might turn important when inverting splitting data to retrieve fluid flow velocity. Conversely, the short chirp strategy targeting a single mode provides a limited information on the flow. It therefore appears interesting to combine the two strategies, which is what we have done. From the first strategy, we obtained first-step splitting data for a large collection of doublets (typically ~ 50), covering all libration phases (typically from 0 to 360° in 36° steps). We then extracted the raw acoustic signals and the corresponding played chirp segment around the time at which these doublets were excited. These short signals were then analyzed with our high-resolution technique. The main difference with the direct short-chirp strategy is the contamination of the records by remnants of other resonances than the targeted doublet.

Figure 9 shows a few examples of the results we obtain. The first example, for the ${}_0S_2^1$ doublet, shows two frequencies that are very precisely retrieved, fitting Greenspan's prediction within less than 0.2 Hz, the higher frequency singlet being less prominent. The detections around 950 Hz are from the ${}_0S_2^2$ doublet.

In the second example, for ${}_0S_4^1$, the recovered dominant frequencies appear shifted by some 15 Hz from the expected values. It could be due to the interference with the neighbouring ${}_0S_4^2$ doublet.

For the ${}_0S_5^5$ doublet, the lower frequency is well retrieved but one cannot clearly identify the frequency of the second singlet.

The last example (mode ${}_3S_3^3$) yields good results, but spurious hits might render the proper identification difficult.

Our tests show that this combined strategy can give good results, allowing for a higher precision, when the number of intervening frequencies is limited, but is unsuccessful when many modes are present within the considered time-window. A more evolved treatment along the same lines could probably yield better results.

3.4 Acoustic mode splitting collection

Using the phase-shifted long chirp strategy, we were able to measure the splitting of 53 identified doublets, with frequencies between 500 and 5 000 Hz, from multiplet ${}_0S_1$ to multiplets ${}_0S_{14}$, ${}_1S_{10}$, ${}_2S_5$ and ${}_3S_4$, for almost all libration phases.

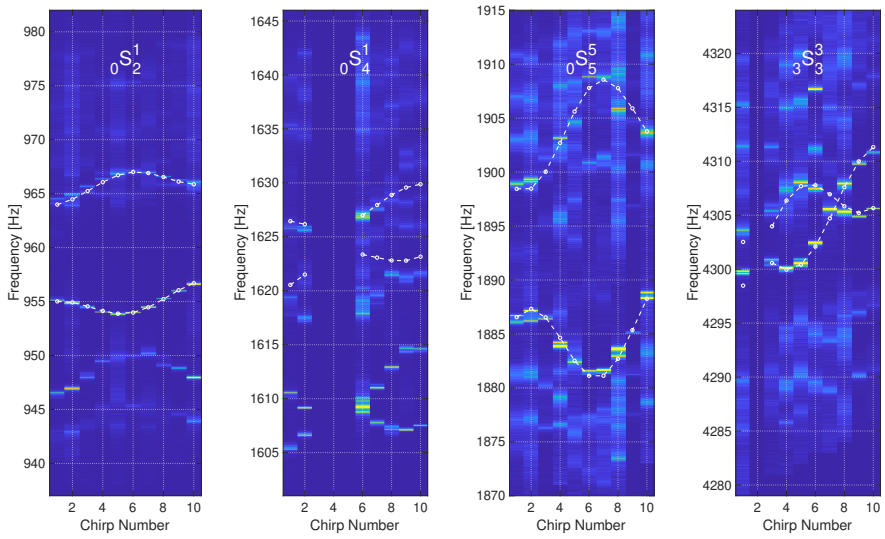

Fig. 9 Examples of results obtained with the combined long chirps-high resolution strategy. As in Figure 7, the color maps are composites of 10 stripes corresponding to 10 successive libration phases (x-axis). Each stripe gives the probability that a given frequency (y-axis) is present in the piece of record analyzed by the high-resolution algorithm. Uniform blue stripes when no data is available. The white dashed lines and circles are the predictions obtained by convolving Greenspan's geostrophic azimuthal flow with the acoustic splitting kernel. From left to right: ${}_0S^1_2$, ${}_0S^1_4$, ${}_0S^5_5$, and ${}_3S^3_3$ doublets. The trend towards larger frequency for larger libration number is due to the warming up of the gas inside ZoRo. It is taken into account in the predictions.

Figure 10 shows an example of splittings measured for a libration phase of 180° (by least-square sine interpolation of the data at 10 libration phases), with $f_o = 15$ Hz, $f_{lib} = 0.05$ Hz and $\Delta f = 1.5$ Hz. Overtone ($n > 0$) spectral peaks are usually much more narrow than those of fundamentals ($n = 0$), yielding smaller splitting error bars. These data are used in a companion article (Nataf and Su 2025) that focuses on the inversion of such data to recover fluid flow.

4 Limitations and perspectives

So far, the value of Modal Acoustic Velocimetry for mapping fluid flows in gas-filled containers was only demonstrated for steady or statistically steady flows (Triana et al. 2014; Mautino 2016; Su et al. 2020; Su 2020). We have presented and tested two different strategies to acquire acoustic data in a gas-filled container when the gas experiences a non-stationary flow. Our first strategy only applies to time-periodic flows. By playing a suite of long chirps that are offset by an increasing phase lag with respect to the periodic flow, we can retrieve the frequency splitting of a large collection of acoustic doublets (typically 60) from each spectra of the suite. We can therefore sample the flow at different phases and get a rather complete flow map by inversion, given the large number of recovered doublets.

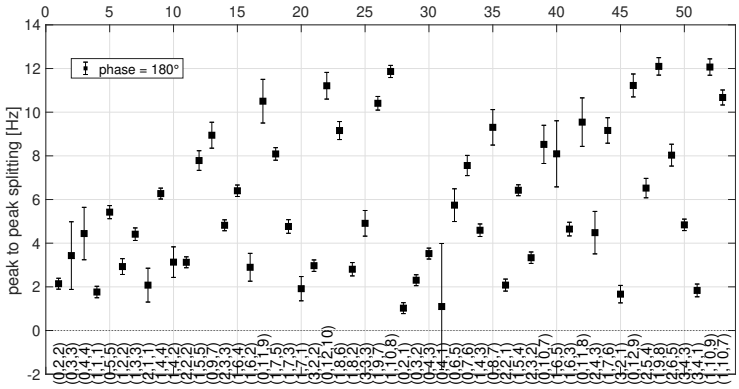

Fig. 10 Measured peak-to-peak splitting (in Hz) of 53 doublets, labeled along the x-axis by their $(n, l, |m|)$ index triplet. Libration-driven flow at a phase of 180°, with $f_o = 15$ Hz, $f_{lib} = 0.05$ Hz and $\Delta f = 1.5$ Hz.

Our second strategy relies on playing a succession of very short chirps that can follow the flow evolution. Non-periodic flows can thus be monitored, but only through their signature on a limited number of acoustic doublets (typically 1 to 4). The high-resolution algorithm we developed provides a much higher resolution of the frequency splitting than the classical measurement from the power spectra.

In both cases, we have observed that a given acoustic mode samples the flow at a time delayed by of a few tenths of a second after its eigenfrequency is played. We think that it is due to the time it takes for a mode to build up, but this point would need further analyses. As a matter of fact, libration-induced flows provide an interesting and original tool for probing the buildup process of a large collection of acoustic modes.

Although the acquisition of the data is quite fast, its post-processing is rather time-consuming, requiring visual inspection of the spectra for reliable mode identification and splitting measurement. Su et al. (2020) have shown how to build very realistic synthetic spectra. The prediction of libration flows is also very reliable. One can therefore envision more automated or artificial intelligence-based processing.

The focus of our present article is rather methodological. We hope it opens the way to a broader experimental study of libration or precession flows in more exotic regimes.

5 Conclusion

We present the first application of Modal Acoustic Velocimetry to time-varying fluid flows. Focusing on periodic libration-induced flows, we have proposed and tested two acquisition strategies.

The first one rests on exciting a large collection of acoustic modes by playing long-duration chirps (typically 100s) spanning a large frequency range (typically from 500 to 5 000 Hz) in order to obtain a good spectral resolution (typically 0.01 Hz) of the resonance peaks, and thus of the frequency splitting produced by the flow. By playing such chirps several times (typically 10 times) starting at successive phases of

the libration-induced flow, we can recover the time-evolution of the flow. The trick being to relate the time at which a given acoustic doublet is excited to the libration phase at that instant.

The second strategy targets individual doublets, which we excite by a succession of short chirps (typically spanning 80 Hz in 0.4s). Each chirp probes a different phase of libration. For such a short chirp, a standard power spectrum is not efficient at resolving the frequency splitting of the doublet. But its duration is long enough for hundreds of cycles to be played and recorded. We thus apply a high-resolution algorithm that tests for the presence of a limited number of monochromatic components and yields the two dominant frequencies, corresponding to the individual singlets.

Both methods yield mode splittings that agree very well with the predictions derived from Greenspan's theory (Greenspan 1968). However, we observe a small unexpected delay, which we attribute to the time needed for the acoustic mode to build up. A detailed study of this delay could bring interesting constraints of this buildup process.

We could acquire the time-evolution of the splitting of 53 acoustic doublets for various libration parameters. A companion article presents the results of 1D- and 2D-inversions of such measurements to recover the time-evolution of the libration-induced fluid flow.

Supplementary information. Supplementary Material provides the audio file example HP0111_per_spe_O15L3T12_3f.wav (30.8 Mo). The file is in the 'WAV' format and contains 11 channels sampled at 44100 Hz on 16 bits. The first eight channels are the signals recorded by 8 microphones situated at a latitude of $\pm 32°$ and different longitudes. Channels 9 and 10 record a libration trigger signal, and a chirp start signal, respectively. Channel 11 records a magnetometer signal used as a rev-counter (see Appendix B for details). The file contains the acoustic response of the ZoRo experiment to a succession of 32 short signals simultaneously played on two loudspeakers at latitudes $+45°$ and $-45°$ along the same meridian. Each of the 32 signals consists in a short chirp, playing frequencies 2 360 to 2 398 Hz in 0.37s, followed by a silence of equal duration. This chirp targets acoustic doublet ${}_1S_3^{\pm 3}$. Libration parameters are: $f_o = 15$ Hz, $f_{lib} = 0.0841$ Hz, and $\Delta f = 1.5$ Hz.

Acknowledgments. This work was partly supported by the Programme National de Planétologie (PNP) of CNRS-INSU co-funded by CNES. DC received funding from the ERC under the European Union's Horizon 2020 research and innovation program via the THEIA project (grant agreement no. 847433). ISTerre is part of Labex OSUG@2020 (ANR10 LABX56).

Declarations

Some journals require declarations to be submitted in a standardised format. Please check the Instructions for Authors of the journal to which you are submitting to see if you need to complete this section. If yes, your manuscript must contain the following sections under the heading 'Declarations':

- Funding This work was partly supported by the Programme National de Planétologie (PNP) of CNRS-INSU co-funded by CNES. DC received funding from the ERC under the European Union's Horizon 2020 research and innovation program via the THEIA project (grant agreement no. 847433). ISTerre is part of Labex OSUG@2020 (ANR10 LABX56).
- Conflict of interest/Competing interests (check journal-specific guidelines for which heading to use) The authors declare no conflict of interest.
- Ethics approval Not applicable.
- Consent to participate
- Consent for publication
- Availability of data and materials
- Code availability
- Authors' contributions The improvements of the ZoRo set-up for this study were conducted by PC, SS, YD and HCN. PR proposed and performed the high-resolution analysis. DC provided Greenspan's flow solution for the spheroid and performed the COMSOL simulations. HCN proposed the long-chirp strategy, performed the runs and their processing. This article was written by HCN, with complements and review by all authors.

If any of the sections are not relevant to your manuscript, please include the heading and write 'Not applicable' for that section.

Editorial Policies for:

Springer journals and proceedings: https://www.springer.com/gp/editorial-policies

Appendix A Libration in a spheroid

Given a longitudinal libration of the spheroid given by equation (1), we derive the expression of the fluid rotation rate $f_{fluid}(s,t)$ in the reference frame of the spinning spheroid. The spheroid being specified by its equatorial r_{eq} and polar r_{pol} radii, we define

$$\frac{f_{Ekman}}{f_o} = \sqrt{\frac{\nu}{2\pi f_o r_{eq}^2}} = \mathrm{Ek}^{1/2} \qquad \text{and} \qquad c = \frac{r_{pol}}{r_{eq}}.$$

The regime of interest is $f_{lib}/f_o \ll 1$ in our case, and the boundary Ekman layers can then be considered as steady. Greenspan and co-workers (Greenspan and Howard 1963; Greenspan 1968) have studied the spin-up of a fluid in axisymmetric containers of geometry $-f(s) \leq z \leq g(s)$. Using equation (5.17) of Greenspan and Howard (1963), we obtain that the expression for $f_{fluid}(s,t)$ is the same as equation (2) for the sphere if the ξ parameter is given by

$$\xi = \frac{f_{lib}}{f_{Ekman}} \frac{f+g}{[1+(f')^2]^{1/4} + [1+(g')^2]^{1/4}}, \tag{A1}$$

where the prime denotes the derivative with respect to the cylindrical radius s. Considering the spheroid geometry $f = g = c(1-s^2)^{1/2}$, we retrieve that ξ^{-1} is given by

equation (A10) of Noir and Cébron (2013), i.e.

$$\xi = \frac{f_{lib}}{f_{Ekman}} \frac{f^{3/2}}{(f^2 + c^4 s^2)^{1/4}} = \frac{f_{lib}}{f_{Ekman}} \frac{c}{[1 - s^2(1 - c^2)]^{1/4}} (1 - s^2)^{3/4}, \tag{A2}$$

where the cylindrical radius s is now normalized by r_{eq}. Since $1 + (f')^2 = f^{-2}$ in the sphere ($c = 1$), ξ is easily formulated in function of the normalized semi-column height $f(s)$. By contrast, equation (A2) cannot be simply derived from the formula in the sphere (equation 2) where the normalized semi-column height f in the sphere would have been replaced by that of the spheroid $f = c(1 - s^2)^{1/2}$. Note finally that the fluid response $f_{fluid}(s, t)$ can also be obtained for any values of f_{lib}/f_o by considering time periodic boundary layers, but at the price of a more complex expression Cébron et al. (2021).

Appendix B Experimental libration diagnostics

Our strategies require sound playing, sound recording, and mechanical driving of the spheroid to be synchronized within a few hundredth of a second. We describe here the steps taken to achieve this goal. The guiding idea is to record synchronization signals together with the acoustic signals on the same data acquisition card, all written is the same wave-format audio file. One typical file thus consists in 11 channels: signals from 8 microphones, a libration nul-phase trigger, a chirp start trigger signal, and a magnetometer signal. The latter is used as a rev-counter: 3 magnets are installed at known longitudes at the equator of the spheroid, yielding a specific signature as they pass in front of a magnetometer chip fixed in the Lab reference frame. An Audacity®screenshot of part of a typical audio file is shown in Figure B1. The complete file is given as Supplementary Material.

Figure B2 illustrates how we exploit the audio files to check the response of the motor to the libration instructions, and to synchronize the acoustic records with the libration record. Time is counted from the start of the audio file. The blue vertical stems mark times at which the libration phase is an integer multiple of 2π, as read from channel 9. The red vertical stems mark chirp starts obtained from channel 10. The blue dots give the instantaneous spin rate of the spheroid computed from the magnetometer signal of channel 11. It can be compared with the requested spin rate (green line) constructed from the libration parameters ($f_o = 15$ Hz, $f_{lib} = 0.084114$ Hz, $\Delta f = 1.5$ Hz) timed by channel 9's trigger.

For this to work, the motor drive should execute the instructions with a minimal delay. The Kollmorgen AKM73Q®motor drive executes instructions sent by a National Instruments real-time compactRIO (cRIO) controller via an EtherCAT®network communication protocol. The requested motor spin rate, and the measured torque and spin rate are exchanged between the cRIO and the servo every 1ms (larger than the 62.5μs lower limit for this protocol). The measured values are averaged over 10 samples. The whole experiment is controlled by a home-made program, written in National Instrument LabVIEW®language, and operated through a multi-tabs user interface running

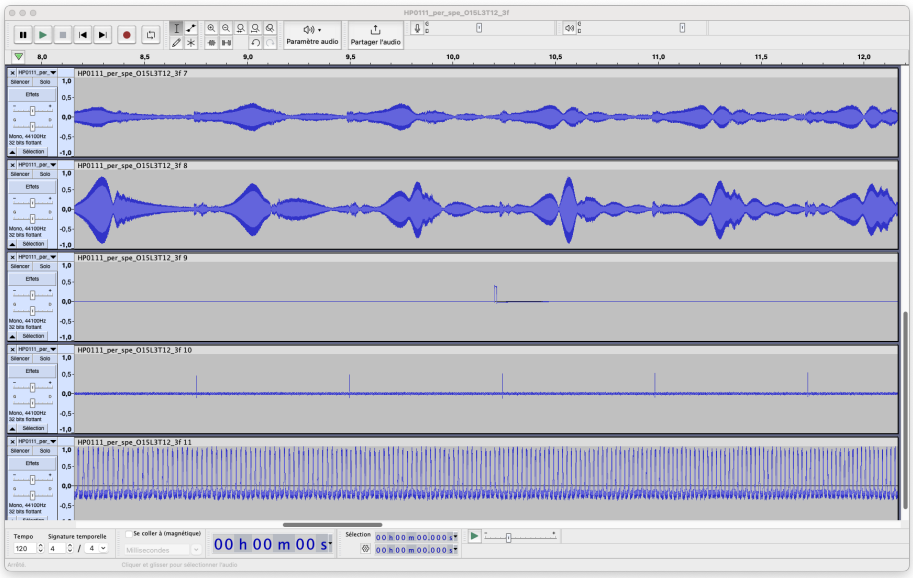

Fig. B1 Audacity®screenshot of part of a typical audio file. Only channels 7 to 11 are shown. Channels 7 and 8 are microphone records. Channel 9 shows one libration nul-phase trigger. Five chirp start triggers are seen on channel 10. Channel 11 records the magnetometer signal that is used as a rev-counter.

on a Windows®Personal Computer (PC) connected to the cRIO via ethernet. All other measurements are retrieved through Data Acquisition Cards connected to this PC.

The PID settings of the motor drive result from a compromise: minimize the time-delay between instructed and achieved spin rate, while keeping the level of instantaneous torque fluctuations low enough to limit noise and allow for large libration amplitudes.

Our acoustic chirps are computed by a Python program and written in a six channels WAV file. The first four channels are the signals sent to each of the four loudspeakers, while the last two only contain a trigger that marks the chirp start. All six channels are played by an ASUS®Xonar DGX audio card in the main PC. Tests reveal that the signals sent by the audio card are delayed by 15ms on channels 5 and 6, and by 5ms on channel 4. These delays are corrected for in the synchronization software. We checked that no delay was introduced on all channels of the TASCAM®US-16x8 Audio/MIDI Interface used to process the microphone signals.

Appendix C Supplementary plots

Figures C3 and C4 show frequency splitting versus libration phase for our collection of 53 acoustic doublets ${}_nS_l^{\pm m}$. ZoRo is filled with nitrogen at atmospheric pressure. Libration parameters are: $f_o = 15$ Hz, $f_{lib} = 0.05$ Hz and $\Delta f = 1.5$ Hz. Chirps played from 500 to 5 000 Hz in 82s. Measured splittings are plotted with their error bars. The dashed lines are sine-interpolations of the measurements. The solid lines

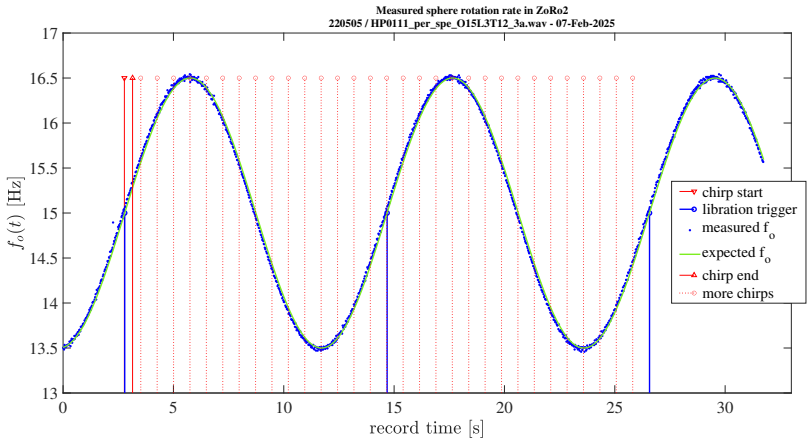

Fig. B2 Example of libration diagnostics. Instantaneous spinning rate of the spheroid as a function of time. The blue vertical stems mark times at which the libration phase is an integer multiple of 2π. The red vertical stems mark chirp starts. The blue dots give the instantaneous spin rate of the spheroid computed from the magnetometer signal. It can be compared with the requested spin rate (green line) constructed from the libration parameters ($f_o = 15$ Hz, $f_{lib} = 0.084114$ Hz, $\Delta f = 1.5$ Hz). ¡

are predictions obtained by convolving the geostrophic azimuthal flow of Greenspan's theory with the splitting kernel of each acoustic doublet.

Appendix D High-resolution algorithm

Many theoretical, numerical, and experimental works have been performed on the determination of discrete frequencies in a multi-tone audible signal that can be generalized to a complex spectrum search (Kay and Marple 1981). High-resolution methods were developed such as the multiple signal classification (MUSIC) technique (Rajan and Bhatta 1993; Candy and Sullivan 1989; Chouhan and Anand 1993; Krasny and Antonyuk 1997), the Prony method (Shang et al. 1988), and the more sophisticated ESPRIT algorithm (Roy and Kailath 1989; Roy et al. 2003). This latter approach is similar to the more general matrix-pencil method (Hua and Sarkar 1990; Laroche 1993).

The originality of IRWIN (Roux et al. 2004; Philippe et al. 2008) is to combine a modified Prony method (Scharf and Demeure 1991) with an iterative approach that looks for the frequency occurrence when different sets of data points are chosen within the time record.

We present here the main steps of the algorithm. We assume that the acoustic pressure field recorded at a given microphone is dominated by M monochromatic signals. Naming δt the sampling time step of the record, we can express the time-record $P(n)$ over a time-window $n\delta t$ as:

$$P(n) = \sum_{m=1}^{M} \tilde{a}_m \left[\exp\left(i\omega_m \delta t\right)\right]^n = \sum_{m=1}^{M} \tilde{a}_m z_m^n, \tag{D3}$$

where ω_m is the angular frequency of the m monochromatic component, and $\tilde{a}_m$ its amplitude. Our goal is to identify the components z_m of largest amplitude from a collection of time-windows with increasing number of points n, *i.e.* solving the following set of equations:

$$\begin{cases} P(0) &= \tilde{a}_1 + \tilde{a}_2 + ... + \tilde{a}_M \\ P(1) &= \tilde{a}_1 z_1 + \tilde{a}_2 z_2 + ... + \tilde{a}_M z_M \\ ... & \\ P(M-1) &= \tilde{a}_1 z_1^{M-1} + \tilde{a}_2 z_2^{M-1} + ... + \tilde{a}_M z_M^{M-1} \\ ... & \\ P(2M-1) &= \tilde{a}_1 z_1^{2M-1} + \tilde{a}_2 z_2^{2M-1} + ... + \tilde{a}_M z_M^{2M-1} \end{cases} \tag{D4}$$

The first step is to symbolically invert the first M equations of this system to express amplitudes $\tilde{a}_1$ to $\tilde{a}_M$ as a function of the data $P(0)$ to $P(M-1)$ and of the phases z_1 to z_M. Replacing $\tilde{a}_1$ to $\tilde{a}_M$ in the last M equations, one obtains a system that is strongly non-linear in the variables z_m but linear in the Elementary Symmetric Polynomials (*ESP*) E_m of the z_m unknowns, given by:

$$E_1 = \sum_{i=1}^{M} z_i, E_2 = \sum_{i=1}^{M} \sum_{j=i+1}^{M} z_i z_j, ..., E_M = \pi_{i=1}^{M} z_i. \tag{D5}$$

One thus recovers the following set of linear equations:

$$\begin{cases} P(M) &= P(M-1)E_1 - P(M-2)E_2 + ... + (-1)^{M-1} P(0) E_M \\ P(M+1) &= P(M)E_1 - P(M-1)E_2 + ... + (-1)^{M-1} P(1) E_M \\ & ... \\ P(2M-1) &= P(2M-2)E_1 - P(2M-3)E_2 + ... + (-1)^{M-1} P(M-1) E_M \end{cases} \tag{D6}$$

The *ESP* are then easily obtained. The unknowns z_m are obtained as the roots of a polynomial of degree M whose coefficients are the *ESP* E_1 to E_M.

Appendix E Acoustic mode buildup

Both strategies we developed rely on the capture of the flow by a given acoustic mode. When the flow is time-dependent, the question is: when does the mode capture the flow? The results presented in sections 3.1 and 3.2 both indicate that this capture occurs a few tenths of a second after the resonance peak frequency of the mode is played. Here, we show that this is comparable to the time it takes for a mode to build up or to fade away.

We tested mode buildup by first identifying the resonant frequency of a few modes, playing 10s-long monochromatic sounds, with a step-by-step frequency increase of 1 Hz. The frequency yielding the largest amplitude is the resonant frequency. We then played a sine signal at this frequency for 10s, and observed the raise of the response on our microphone array.

Figure E5 shows the growth and decay of mode ${}_1S_3^3$ at one microphone. The envelope of the signals can be fit by $1-\exp(-t/\tau)$ and $\exp(-t/\tau)$ functions (Trusler 1991, p.219), defining buildup time τ. In the ZoRo experiment at rest, our measurements

yield buildup times $\tau = 0.30$, 0.22, and 0.20s for modes ${}_0S_2^2$, ${}_1S_3^3$ and ${}_2S_1^0$, respectively. We have not conducted a systematic survey of these buildup times, and the effect of the rotation, of playing a chirp, and of the convolution with the time-varying flow remain to be explored. However, this analysis supports our interpretation of the observed time-delay of our observation with respect to Greenspan's prediction as being due to mode buildup.

References

Aerts, C., Christensen-Dalsgaard, J., Kurtz, D.W.: Asteroseismology. Springer, Dordrecht Heidelberg London New York (2010)

Albo, P.G., Gavioso, R., Benedetto, G.: Modeling steady acoustic fields bounded in cavities with geometrical imperfections. International Journal of Thermophysics **31**(7), 1248–1258 (2010)

Aldridge, K.D.: An experimental study of axisymmetric inertial oscillations of a rotating liquid sphere. PhD thesis, Massachusetts Institute of Technology (1967)

Busse, F.H.: Mean zonal flows generated by librations of a rotating spherical cavity. Journal of Fluid Mechanics **650**, 505–512 (2010)

Chouhan, H.M., Anand, G.: Normal mode wave-number estimation using a towed array. The Journal of the Acoustical Society of America **93**(4), 1807–1814 (1993)

Comstock, R.L., Bills, B.G.: A solar system survey of forced librations in longitude. Journal of Geophysical Research: Planets **108**(E9) (2003)

Candy, J.V., Sullivan, E.J.: Model-based passive ranging. The Journal of the Acoustical Society of America **85**(6), 2472–2480 (1989)

Cébron, D., Vidal, J., Schaeffer, N., Borderies, A., Sauret, A.: Mean zonal flows induced by weak mechanical forcings in rotating spheroids. Journal of Fluid Mechanics **916**, 39 (2021)

Deleplace, B.: Eddy viscosity in rotating fluids: an experimental study - Consequences on the visco-magnetic torque at the Core Mantle Boundary (CMB). Theses, Université Joseph-Fourier - Grenoble I (October 2005). https://tel.archives-ouvertes.fr/tel-00012097

Greenspan, H., Howard, L.: On a time-dependent motion of a rotating fluid. Journal of fluid mechanics **17**(3), 385–404 (1963)

Greenspan, H.P.: The Theory of Rotating Fluids. Cambridge Monographs on Mechanics and Applied Mathematics. Cambridge University Press, Cambridge, UK (1968)

Hua, Y., Sarkar, T.K.: Matrix pencil method for estimating parameters of exponentially damped/undamped sinusoids in noise. IEEE Transactions on Acoustics, Speech, and Signal Processing **38**(5), 814–824 (1990)

Krasny, L.G., Antonyuk, S.P.: Wave-number estimation in an ocean waveguide. The Journal of the Acoustical Society of America **102**(5), 2697–2704 (1997)

Kay, S.M., Marple, S.L.: Spectrum analysis—a modern perspective. Proceedings of the IEEE **69**(11), 1380–1419 (1981)

Kaplan, E.J., Schaeffer, N., Vidal, J., Cardin, P.: Subcritical thermal convection of liquid metals in a rapidly rotating sphere. Phys. Rev. Lett. **119**, 094501 (2017) https://doi.org/10.1103/PhysRevLett.119.094501

Laroche, J.: The use of the matrix pencil method for the spectrum analysis of musical signals. The Journal of the Acoustical Society of America **94**(4), 1958–1965 (1993)

Le Bars, M., Cébron, D., Le Gal, P.: Flows driven by libration, precession, and tides. Annual Review of Fluid Mechanics **47**, 163–193 (2015)

Ledoux, P.: The nonradial oscillations of gaseous stars and the problem of Beta Canis Majoris. Astrophysical Journal **114** (1951)

Mautino, A.R.: Inverse spectral methods in acoustic normal mode velocimetry of high Reynolds number spherical Couette flows. Master's thesis, University of Maryland (2016)

Mehl, J.B.: Acoustic eigenvalues of a quasispherical resonator: second order shape perturbation theory for arbitrary modes. Journal of research of the National Institute of Standards and Technology **112**(3), 163 (2007)

Moldover, M.R., Mehl, J.B., Greenspan, M.: Gas-filled spherical resonators: Theory and experiment. The Journal of the Acoustical Society of America **79**(2), 253–272 (1986)

Noir, J., Cébron, D.: Precession-driven flows in non-axisymmetric ellipsoids. Journal of Fluid Mechanics **737**, 412–439 (2013)

Noir, J., Hemmerlin, F., Wicht, J., Baca, S.M., Aurnou, J.M.: An experimental and numerical study of librationally driven flow in planetary cores and subsurface oceans. Physics of the Earth and Planetary Interiors **173**(1-2), 141–152 (2009) https://doi.org/10.1016/j.pepi.2008.11.012

Nataf, H.-C., Su, S.: Modal Acoustic Velocimetry in libration-driven flows - Part 2 : Flow inversion. to be submitted (2025)

Philippe, F.D., Roux, P., Cassereau, D.: Iterative high-resolution wavenumber inversion applied to broadband acoustic data. IEEE transactions on ultrasonics,

ferroelectrics, and frequency control **55**(10), 2306–2311 (2008)

Rajan, S.D., Bhatta, S.D.: Evaluation of high-resolution frequency estimation methods for determining frequencies of eigenmodes in shallow water acoustic field. The Journal of the Acoustical Society of America **93**(1), 378–389 (1993)

Roux, P., Cassereau, D., Roux, A.: A high-resolution algorithm for wave number estimation using holographic array processing. The Journal of the Acoustical Society of America **115**(3), 1059–1067 (2004)

Roy, R., Kailath, T.: ESPRIT-estimation of signal parameters via rotational invariance techniques. IEEE Transactions on acoustics, speech, and signal processing **37**(7), 984–995 (1989)

Roy, R., Paulraj, A., Kailath, T.: ESPRIT–a subspace rotation approach to estimation of parameters of cisoids in noise. IEEE transactions on acoustics, speech, and signal processing **34**(5), 1340–1342 (2003)

Schaeffer, N.: Efficient spherical harmonic transforms aimed at pseudospectral numerical simulations. Geochemistry, Geophysics, Geosystems **14**(3), 751–758 (2013)

Su, S., Cébron, D., Nataf, H.-C., Cardin, P., Vidal, J., Solazzo, M., Do, Y.: Acoustic spectra of a gas–filled rotating spheroid. European Journal of Mechanics-B/Fluids **84**, 302–310 (2020)

Scharf, L.L., Demeure, C.: Statistical signal processing: detection, estimation, and time series analysis. (No Title) (1991)

Su, S.: Modal Acoustic Velocimetry in a gas–filled rotating spheroid. Theses, Université Grenoble Alpes [2020-....] (February 2020). https://theses.hal.science/tel-02612799

Shang, E., Wang, H., Huang, Z.: Waveguide characterization and source localization in shallow water waveguides using the Prony method. The Journal of the Acoustical Society of America **83**(1), 103–108 (1988)

Tilgner, A.: Driven inertial oscillations in spherical shells. Physical Review E **59**(2), 1789 (1999)

Trusler, M.: Physical Acoustics and Metrology of Fluids. CRC Press, ??? (1991)

Triana, S.A., Zimmerman, D.S., Nataf, H.-C., Thorette, A., Lekic, V., Lathrop, D.P.: Helioseismology in a bottle: Modal Acoustic Velocimetry. New Journal of Physics **16**(11), 113005 (2014)

Vidal, J., Su, S., Cebron, D.: Compressible fluid modes in rigid ellipsoids: towards modal acoustic velocimetry. Journal of Fluid Mechanics **885** (2020)

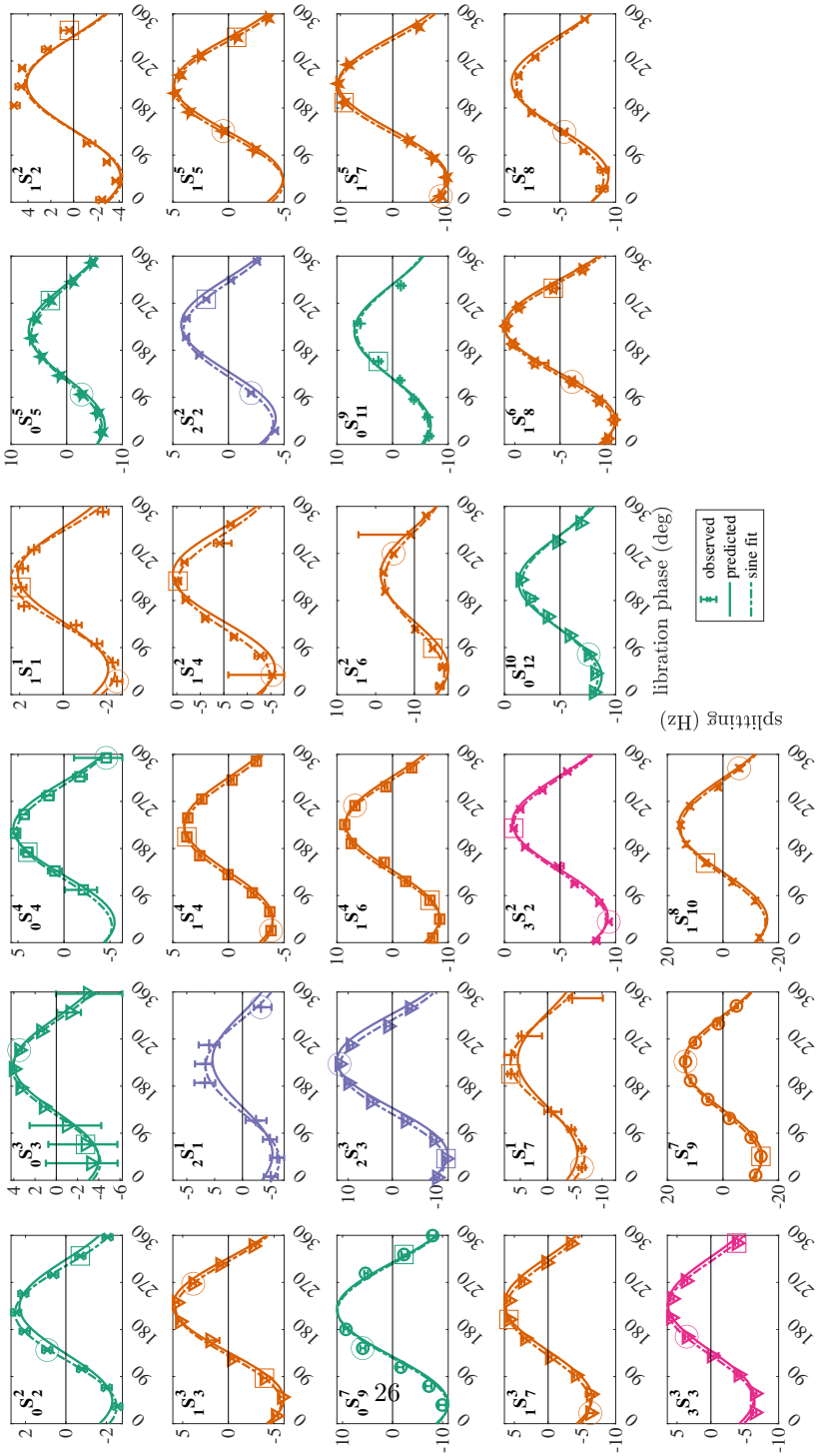

Fig. C3 Frequency splitting (in Hertz) versus libration phase (in degrees) for 27 equatorially symmetric ${}_nS_l^{|m|}$ doublets. Libration parameters: $f_o = 15$ Hz, $f_{lib} = 0.05$ Hz and $\Delta f = 1.5$ Hz. From ten phase-offset 82s-long chirps. Solid line: splitting prediction from Greenspan's theory. Dashed line: least-square sine fit to measured splittings.

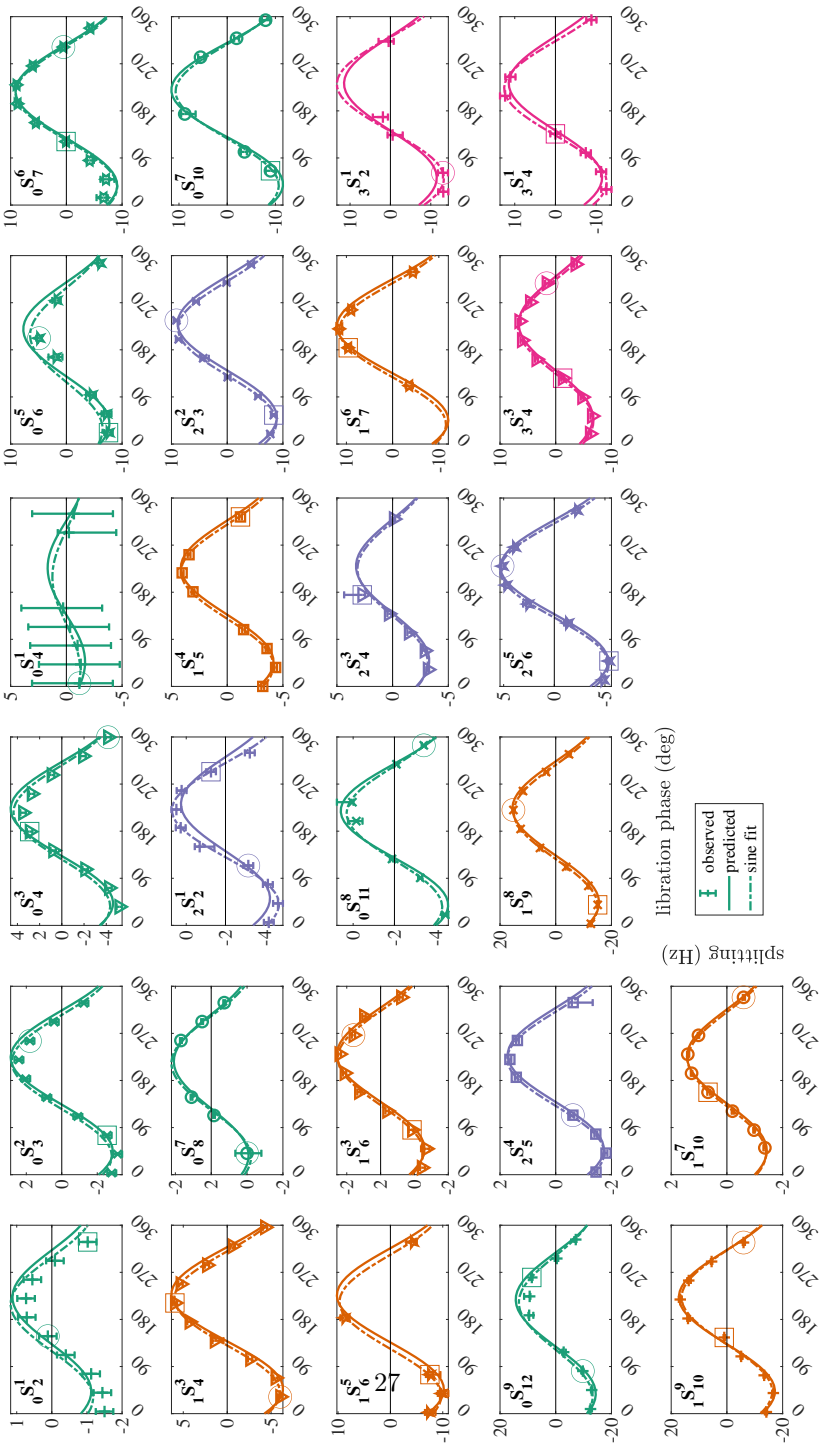

Fig. C4 Same as Figure C3 for 26 equatorially anti-symmetric ${}_nS_l^{|m|}$ doublets.

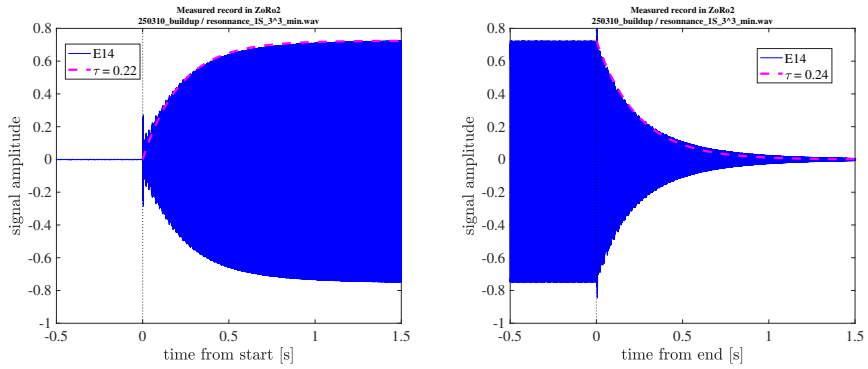

Fig. E5 An example of mode buildup and decay. Doublet ${}_1S_3^3$ was excited, by playing a 10s-long monochromatic sound at its resonance frequency of 2362 Hz. The record at one of the microphones is displayed. (a) Zoom on the growth of the acoustic mode. (b) Zoom on its decay. The envelopes are well fit by $1 - \exp(-t/\tau)$ and $\exp(-t/\tau)$ (magenta dashed lines) with $\tau = 0.22$ and $\tau = 0.24$, respectively.